Ataxia Telangiectasia Mutated and MSH2 Control Blunt DNA End Joining in Ig Class Switch Recombination

Emily Sible,[*,†] **Mary Attaway,**[†] **Giuseppe Fiorica,**[†] **Genesis Michel,**[†] **Jayanta Chaudhuri,**[‡] **and Bao Q. Vuong**[*,†]

Class-switch recombination (CSR) produces secondary Ig isotypes and requires activation-induced cytidine deaminase (AID)–dependent DNA deamination of intronic switch regions within the IgH (*Igh*) gene locus. Noncanonical repair of deaminated DNA by mismatch repair (MMR) or base excision repair (BER) creates DNA breaks that permit recombination between distal switch regions. Ataxia telangiectasia mutated (ATM)–dependent phosphorylation of AID at serine 38 (pS38-AID) promotes its interaction with apurinic/apyrimidinic endonuclease 1 (APE1), a BER protein, suggesting that ATM regulates CSR through BER. However, pS38-AID may also function in MMR during CSR, although the mechanism remains unknown. To examine whether ATM modulates BER- and/or MMR-dependent CSR, $Atm^{-/-}$ mice were bred to mice deficient for the MMR gene mutS homolog 2 (*Msh2*). Surprisingly, the predicted Mendelian frequencies of $Atm^{-/-}Msh2^{-/-}$ adult mice were not obtained. To generate ATM and MSH2-deficient B cells, *Atm* was conditionally deleted on an $Msh2^{-/-}$ background using a floxed ATM allele (Atm^{f}) and B cell–specific Cre recombinase expression (*CD23-cre*) to produce a deleted ATM allele (Atm^{D}). As compared with $Atm^{D/D}$ and $Msh2^{-/-}$ mice and B cells, $Atm^{D/D}Msh2^{-/-}$ mice and B cells display a reduced CSR phenotype. Interestingly, Sμ–Sγ1 junctions from $Atm^{D/D}Msh2^{-/-}$ B cells that were induced to switch to IgG1 in vitro showed a significant loss of blunt end joins and an increase in insertions as compared with wild-type, $Atm^{D/D}$, or $Msh2^{-/-}$ B cells. These data indicate that the absence of both ATM and MSH2 blocks nonhomologous end joining, leading to inefficient CSR. We propose a model whereby ATM and MSH2 function cooperatively to regulate end joining during CSR through pS38-AID. *The Journal of Immunology*, 2023, 210: 369–376.

B cells recognize and eliminate Ags by producing Igs, also known as Abs. Each Ig is composed of two H chain (IgH) and two L chain (IgL) polypeptides, which are held together by disulfide bonds to form the characteristic "Y" shape structure of the Ig (1). The N termini of IgH and IgL comprise the variable region of each polypeptide, and together they form the Ag binding site of the Ig, whereas the C region of IgH imparts the effector function of the Ig.

In a process known as class-switch recombination (CSR), mature B cells generate dsDNA breaks (DSBs) within the IgH gene locus (*Igh*) to diversify the Ig repertoire through a DNA recombination event and produce new Ig isotypes (2–4). CSR is mediated by the enzymatic activity of activation-induced cytidine deaminase (AID) (5–7), which converts deoxycytidines into deoxyuridines in the repetitive switch (S) region that precedes each *Igh* constant coding exon (5–7). Noncanonical repair of these U:G mutations in DNA by either mismatch repair (MMR) or base excision repair (BER) creates staggered DNA breaks that promote recombination between distal S regions (8–15) and expression of alternative *Igh* constant coding exons.

During BER, uracil DNA glycosylase (UNG) generates an abasic site by removing the AID-generated uracil base, allowing for subsequent cleavage of the phosphodiester backbone by apurinic/apyrimidinic

endonuclease 1 (APE1) to generate an ssDNA break (SSB) (13, 16). In contrast, MMR utilizes a heterodimer of mutS homologs mutS homolog 2 (MSH2) and MSH6 to recognize DNA base pair mismatches and recruit the mutL homology 1 (MLH1) and PMS1 homolog 2 (PMS2) heterodimer to cleave the phosphodiester backbone 5′ of the mismatch (6). Exonuclease-1 (EXO1) degrades the DNA to remove the U:G mismatch (17). Staggered SSBs in close proximity constitute DSBs, which are converted into recombination events. Mice deficient in MSH2 or UNG show reduced levels of switched isotypes as compared with wild-type (WT) mice (8). Furthermore, simultaneous loss of both MSH2 and UNG blocks CSR completely, demonstrating the complementary function of MMR and BER in CSR (8).

Activation of BER and MMR during CSR is mediated by the phosphorylation of AID at serine 38 (pS38-AID), which promotes the interaction of AID with APE1 (18). Mice with a homozygous knock-in mutation of the phosphorylation site ($Aicda^{S38A/S38A}$), which changes S38 to an alanine, have significantly reduced CSR (19, 20). $Aicda^{S38A/S38A}$ mice with homozygous null mutations in *Ung* or *Msh2* show a CSR phenotype comparable to $Ung^{-/-}Msh2^{-/-}$ mice, indicating a critical role of AID phosphorylation in activating BER and MMR during CSR (21). Furthermore, AID phosphorylation at S38 requires ataxia telangiectasia mutated (ATM), a PI3K-related kinase

*Biology PhD Program, The Graduate Center, The City University of New York, New York, NY; †Department of Biology, City College of New York, The City University of New York, New York, NY; and ‡Memorial Sloan Kettering Cancer Center, New York, NY

ORCIDs: 0000-0002-3838-0075 (J.C.); 0000-0001-5416-9635 (B.Q.V.).

Address correspondence and reprint requests to Prof. Bao Q. Vuong, The City College of New York, 160 Convent Avenue, Marshak 526, New York, NY 10031. E-mail address: bvuong@ccny.cuny.edu

The online version of this article contains supplemental material.

Abbreviations used in this article: A-EJ, alternative end joining; AID, activation-induced cytidine deaminase; APE1, apurinic/apyrimidinic endonuclease 1; ATM, ataxia telangiectasia mutated; BER, base excision repair; CSR, class-switch recombination; DNA-PKcs, DNA-dependent protein kinase catalytic subunit; DSB, dsDNA break; E13.5, embryonic day 13.5; EXO1, exonuclease 1; MMR, mismatch repair; pS38-AID, phosphorylation of AID at serine 38; MSH2, mutS homolog 2; NHEJ, nonhomologous end joining; NP-CGG, 4-hydroxy-3-nitrophenylacetyl conjugated to chicken γ globulin; P0, postnatal day 0; P28, postnatal day 28; ROS, reactive oxygen species; S, switch; SSA, single strand annealing; SSB, ssDNA break; UNG, uracil DNA glycosylase; WT, wild-type; XRCC4, X-ray repair cross complementing 4.

(PIKK) that responds to DSBs and is required for WT CSR (22, 23). $Atm^{-/-}$ mice show reduced levels of pS38-AID and impaired AID/APE1 interaction, suggesting that ATM promotes phosphorylation of AID to induce its interaction with APE1 and drive CSR through BER (18). However, the mechanism by which ATM signals noncanonical, recombinogenic BER during CSR remains unclear.

After BER- and MMR-dependent DSBs are formed in the recombining S regions, nonhomologous end joining (NHEJ) factors ligate the broken ends and promote DNA recombination rather than canonical DSB repair (24, 25). Notably, the absence of NHEJ factors, such as Ku70, Ku80, X-ray repair cross complementing 4 (XRCC4), or DNA ligase IV, reduces CSR efficiency and increases *Igh* chromosomal translocations (26–28). Without NHEJ, CSR can be completed through a microhomology-mediated end joining pathway, also known as alternative end joining (A-EJ), which is more error-prone and less efficient than NHEJ (29, 30). Recombined S−S junctions from WT B cells show ligations resulting primarily from NHEJ (26, 27). Most of these NHEJ-repaired S−S junctions show short stretches of homology, or microhomology, between donor and acceptor S regions of <4 nt, and the remaining ~30% of S−S junctions contain no homology between the recombining S regions and are characterized as a blunt end join (31). Recombined S−S regions that have been repaired by A-EJ contain longer stretches of homology, which skew toward ≥5 nt (26, 31), yet the conditions under which A-EJ is favored over NHEJ during CSR remain unclear. $Atm^{-/-}$ B cells exhibit longer microhomologies in recombined S−S junctions, indicating that ATM is required for NHEJ, and A-EJ mediates recombinational repair in the absence of ATM (23, 32). Interestingly, MSH2 has been implicated in regulating A-EJ during CSR because Sμ−Sγ3 junctions from B cells lacking MSH2 exhibited no microhomology above 5 nt (10). In this study, we demonstrate an epistatic role for *Atm* to *Msh2* in CSR. Loss of MSH2 and ATM in B cells leads to a reduction in CSR concurrent with a block in blunt-end S−S junctions, suggesting a role for MSH2 in enforcing NHEJ in the absence of ATM. Additionally, to our knowledge, we report a novel synthetic lethality between *Atm* and *Msh2*, which implicates ATM or MSH2 as a potential therapeutic target for cancers driven by mutations in either gene.

Materials and Methods
Mice

C57BL/6 and $Atm^{-/-}$ (stock no. 008536) mice were purchased from The Jackson Laboratory (33). $Msh2^{-/-}$ mice were a gift from H. te Riele (34), $Aicda^{-/-}$ mice were a gift from T. Honjo (35), $Atm^{fl/fl}$ mice were a gift of Shan Zha (36), and *CD23-Cre* mice were a gift of Meinrad Busslinger (37). Husbandry of and experiments with mice were conducted according to protocols approved by The City College of New York Institutional Animal Care and Use Committee.

Genotyping of mice and embryos

To obtain embryonic day 13.5 (E13.5) embryos, females 3–6 mo of age were placed into a cage previously occupied by male mice 1 d prior to introducing the male mouse. Timed matings were set up by limiting the mating period to 1 d. Pregnant female mice were euthanized 14 d after mating (E13.5), and embryos were collected from the uterine horn immediately after euthanasia. To genotype the embryos, one hindlimb and tail were incubated in lysis buffer (10 mM Tris, 0.1 M EDTA, 0.5% SDS, and 200 μg/ml proteinase K) overnight at 56°C. Genomic DNA was isolated by isopropanol precipitation and resuspended in TE buffer. To genotype newborn mice (postnatal day 0 [P0]), pregnant females were monitored daily for neonates ~3 wk after mating. Tail biopsies were collected from neonates for genotyping. When a dead carcass or stillborn neonate was found in the litter, tissue samples or tail biopsies were collected and genotyped when possible. Adult mice were identified by tail biopsy ~4 wk after birth (postnatal day 28 [P28]), when the mice were weaned from the nursing female. The primers for each genotype are as follows: *Atm* (ATMB, 5′-CGAATTTGCAGGAGTTGCTGAG-3′; ATMF, 5′-GACTTCTGTCAGATGTTGCTGCC-3′; and ATMN,

5′-GGGTGGGATTAGATAAATGCCTG-3′), *Msh2* (MshF, 5′-GCTCACTTAGACGCCATTGT-3′; MshWR, 5′-AAAGTGCACGTCATTTGGA-3′; and MshKR, 5′-GCCTTCTTGACGAGTTCTTC-3′), CD23-Cre (CD23cre_1, 5′-GCGACTAGTAACTTGTTTATTGCA GCTTAT-3′; and CD23cre_2, 5′-GCGTCCGGAAGACACCCACATCCCAATTCTT-3′), and Atm^f (ATMgF86723, 5′-ATCAAATGTAAAGGCGGCTTC-3′; ATM_BAC13, 5′-CATCCTTTAATGTGCCTCCCTTCGCC-3′; and ATM_BAC7, 5′-GCCCATCCCGTCCACAAT ATCTCTGC-3′). PCR with DreamTaq (Thermo Fisher Scientific, no. K1082) was performed for 30 cycles using the following conditions: 95°C, 30 s; melting temperature, 30 s; 72°C, 30 s. The melting temperature (annealing temperature) for *Atm* and *Msh2* was 55°C, CD23-Cre 58°C, and Atm^f 63°C.

B cell purification and stimulation for CSR

B cells were purified from the spleens of mice (aged 2–7 mo of age) through negative selection with anti-CD43 magnetic beads (Miltenyi Biotec) and subsequently cultured in RPMI 1640 media (Life Technologies) supplemented with 10% FBS (Atlanta Biologicals), 2 mM L-glutamine, 1× penicillin/streptomycin (Corning), and 47.3 μM 2-ME. For switching to IgG1, B cells cultured at 1×10^6 cells/ml with 25 μg/ml LPS (Sigma-Aldrich, catalog no. L7261) and 12.5 ng/ml IL-4 (R&D Systems). B cells were split 1:2 (v/v) 48 and 72 h after isolation. To stimulate CSR to IgG3, 25 μg/ml LPS was used. After 96 h poststimulation, B cells were harvested for analysis by flow cytometry. Live cells were kept on ice and stained in Life Technologies PBS (pH 7.4) (catalog no. 10-010-049) supplemented with 2.5% FBS. To identify switched B cells, samples were stained with anti-IgG1 (BD Biosciences; allophycocyanin conjugate, catalog no. BDB550874 or PE conjugate, catalog no. BDB550083) or anti-IgG3 (BD Biosciences; FITC conjugate catalog no. BDB553403). DAPI was used for live/dead exclusion. Samples were analyzed on a BD LSR II cytometer. For proliferation assays, B cells were labeled with carboxylic acid, acetate, succinimidyl ester (SNARF) (Thermo Fisher Scientific, catalog no. S22801) and analyzed by flow cytometry at time of labeling (D0), and every 24 h thereafter.

Immunoblots and RNA expression

Protein extracts were prepared from IgG1-stimulated B cells at 72 h poststimulation. Cells were lysed in Nonidet P-40 lysis buffer supplemented with proteinase inhibitor tablet (MilliporeSigma). Nonidet P-40 cell lysates were resolved on 8% SDS-PAGE gels, transferred overnight to Immobilon (MilliporeSigma), and immunoblotted with anti-ATM (GeneTex, catalog no. GTX70103), anti-MSH2 (Abcam, catalog no. ab70270), anti–α-tubulin (Sigma-Aldrich, catalog no. T9026-100UL) or anti-AID (38) Abs. Immunoblots were developed using anti-mouse HRP or anti-rabbit HRP using the Pierce ECL Western blotting substrate (Thermo Fisher Scientific, catalog no. PI32106) and imaged on an Azure A300 chemiluminescent imaging system. RNA was extracted from IgG1-stimulated B cells at 72 h poststimulation using TRIzol reagent (Thermo Fisher Scientific), and cDNA was prepared using the ProtoScript II kit (NEB). Germline transcription was analyzed using quantitative PCR with SYBR Green (Roche) and primers for Sμ (IμF, 5′-CTCTGGCCCTGCTTATTGTTG-3′; and CμR, 5′-GAAGACATTTGGGAAGGACTGACT-3′) or Sγ1 (Iγ1, 5′-GGCCCTTCCAGATCTTTGAG-3′; and Cγ1, 5′-GGATCCAGAGTTCCAGGTCACT-3′). Reactions were analyzed on a LightCycler 96 (Roche).

Mouse immunizations and Ig titers

Mice (aged 2–6 mo) were injected i.p. with 50 μg of 4-hydroxy-3-nitrophenylacetyl conjugated to chicken γ globulin (NP-CGG) (Biosearch Technologies) in Imject Alum (Thermo Fisher Scientific) (39). Mice were given a boost of NP-CGG in Imject Alum 10 d after primary immunization. Sera were obtained from blood that was collected on day 0 (preimmunization) and day 7 and day 21 (postimmunization) through cheek bleeds (days 0 and 7) or cardiac puncture (day 21). To analyze Ig serum titers, ELISA assays were performed as previously described (21).

S junction analysis

DNA from IgG1-stimulated B cells was isolated from ~1.5×10^6 cells 72 h after stimulation. Sμ–Sγ1 junctions were amplified using nested PCR primers: Sμ1b (5′-AACTCTCCAGCCACAGTAATGACC-3′) and Sγ1.1 (5′-CTGTAACCTACCCAGGAGACC-3′) were used for the first cycle of PCR; SμF2 (5′-GAGAAGGCCAGACTCATAAAGCT-3′) and Sγ1.1R2 (5′-GTCGAATTCCCCCATCCTGTCACCTATA-3′) were used in the second-round PCR, as previously described (40, 41). Both rounds of PCR were performed for an initial 10 cycles at 94°C for 15 s, 52°C for 30 s, and 72°C 2 min, followed by 23 more cycles with 5 s added per cycle. All PCRs were performed using Q5 high-fidelity DNA polymerase (NEB) according to the manufacturer's instructions. Five identical PCR reactions were setup for each B cell stimulation. The reactions were pooled, concentrated in

a speed-vacuum, and resolved on a 1% agarose gel. PCR products (0.5–1 kb) were excised from the gel, cloned into cloning vector pJET1.2 (Thermo Fisher Scientific, catalog no. K1231), and Sanger sequenced using the T7 forward primer. Sequenced junctions were aligned against reference Sμ (MUSIGCD07) and Sγ1 (MUSIGHANB) in National Center for Biotechnology Information BLAST with the low complexity filter disabled.

Figure composition and statistical analysis

Data figures were generated using GraphPad Prism 7.01. Unless otherwise noted, statistical analyses were completed by one-way ANOVA in Prism.

Results

Mutations in Atm and Msh2 induce a developmental lethality late in gestation to early postnatal

BER and MMR function redundantly to direct CSR in B cells (8). ATM regulates the phosphorylation of AID and its interaction with APE1, a BER protein (18). To determine the role of ATM in BER-dependent CSR, we bred $Atm^{-/-}$ and $Msh2^{-/-}$ mice to generate $Atm^{-/-}Msh2^{-/-}$ mice. $Atm^{-/-}$ mice carry a PGKneo modified exon at position 5790 in the Atm locus that recapitulates mutations observed in ataxia telangiectasia patients (33). $Msh2^{-/-}$ mice contain a targeted disruption 5′ of the exon encoding the MSH2 ATP binding domain, resulting in a frameshift and mRNA decay (34). $Atm^{-/-}$ and $Msh2^{-/-}$ single knockout mice survive into adulthood, albeit with mild immune defects and a predisposition to lymphomagenesis (42, 43). Surprisingly, of the 247 mice genotyped at P28, no $Atm^{-/-}Msh2^{-/-}$ mice were found (Table I, $p = 3.3 \times 10^{-4}$), unveiling a novel synthetic lethal relationship. To determine the developmental stage at which the lethality occurs, embryos were collected from timed mating 2 wk after conception (E13.5) and genotyped. Mendelian ratios of E13.5 embryos from a dihybrid cross were obtained (Table II). Newborn pups (P0) from $Atm^{+/-}Msh2^{-/-} \times Atm^{+/-}Msh2^{+/-}$ crosses yielded less than half of the expected number of P0 $Atm^{-/-}Msh2^{-/-}$ neonates; however, these findings are not statistically significant (Table III; $p = 0.292$). Collectively, these data indicate that the $Atm^{-/-}Msh2^{-/-}$ lethality occurs between E13.5 and P0 with an incomplete penetrance of the synthetic lethal phenotype.

CSR is significantly reduced but not ablated in $Atm^{D/D}Msh2^{-/-}$ mice

To examine the function of ATM and MSH2 in CSR, we bred $Msh2^{-/-}$ mice to mice that carry a conditional knockout Atm allele ($Atm^{f/f}$) and transgenic mice expressing Cre recombinase under the control of a B cell–specific promoter ($CD23$-Cre^+) (36, 44). The $CD23$-$Cre^+Atm^{f/f}Msh2^{-/-}$ mice, which carry a conditional deletion of Atm in B cells and a germline deletion of $Msh2$, are hereafter referred to as $Atm^{D/D}Msh2^{-/-}$ mice. Unlike $Atm^{-/-}Msh2^{-/-}$ mice, $Atm^{D/D}Msh2^{-/-}$ mice were obtained at the expected Mendelian frequencies (Supplemental Table I), suggesting that the loss of ATM

Table I. Genotypes of progeny from dihybrid cross at 4 wk postnatal

Cross	N	Genotype	Expected	Observed	χ^2 p Value
$Atm^{+/-}Msh2^{+/-}$	247	$Atm^{+/+}Msh2^{+/+}$	15.44	22	3.3×10^{-4}
×		$Atm^{+/+}Msh2^{+/-}$	30.88	33	
$Atm^{+/-}Msh2^{+/-}$		$Atm^{+/-}Msh2^{+/+}$	30.88	37	
		$Atm^{+/+}Msh2^{-/-}$	15.44	18	
		$Atm^{+/-}Msh2^{+/-}$	61.75	75	
		$Atm^{+/-}Msh2^{-/-}$	30.88	27	
		$Atm^{-/-}Msh2^{+/+}$	15.44	17	
		$Atm^{-/-}Msh2^{+/-}$	30.88	18	
		$Atm^{-/-}Msh2^{-/-}$	15.44	0	

The numbers of expected and observed progeny at postnatal day 28 (P28) from a dihybrid cross are shown. Observed progeny were genotyped at ~4 wk after birth (P28) and represent ≥15 litters. The p value was determined by a χ^2 test.

Table II. Genotypes of progeny from dihybrid cross at midgestation (E13.5)

Cross	N	Genotype	Expected	Observed	χ^2 p Value
$Atm^{+/-}Msh2^{+/-}$	31	$Atm^{+/+}Msh2^{+/+}$	1.9375	2	0.740
×		$Atm^{+/+}Msh2^{+/-}$	3.875	3	
$Atm^{+/-}Msh2^{+/-}$		$Atm^{+/-}Msh2^{+/+}$	3.875	6	
		$Atm^{+/-}Msh2^{+/-}$	7.75	8	
		$Atm^{+/+}Msh2^{-/-}$	1.9375	1	
		$Atm^{+/-}Msh2^{-/-}$	3.875	5	
		$Atm^{-/-}Msh2^{+/+}$	1.9375	1	
		$Atm^{-/-}Msh2^{+/-}$	3.875	2	
		$Atm^{-/-}Msh2^{-/-}$	1.9375	3	

The numbers of expected and observed progeny at embryonic day 13.5 (E13.5) that were obtained in a dihybrid cross from timed matings are shown. Observed progeny were obtained from three or more litters. The p value was determined by a χ^2 test.

and MSH2 in B cells does not contribute to the $Atm^{-/-}Msh2^{-/-}$ lethality. To investigate the loss of ATM and MSH2 on Ig production, $Atm^{D/D}Msh2^{-/-}$ and control mice were immunized with NP-CGG, a T cell–dependent Ag (45, 46). Serum Igs were analyzed by ELISA prior to and 21 d after a primary and booster immunization of NP-CGG. $Atm^{-/-}$, $Aicda^{-/-}$, $Msh2^{-/-}$, and WT mice showed IgM and IgG1 titers that were consistent with previously published reports (Fig. 1) (21, 23, 35, 42). $Atm^{D/D}Msh2^{-/-}$ IgM titers pre- and postimmunization did not differ significantly from WT, $Atm^{-/-}$, $Msh2^{-/-}$, $Atm^{D/D}$, $Msh2^{-/-}$, and $CD23$-Cre^+ mice (Fig. 1). Given that mature B cells produce IgM without undergoing CSR, these data suggest that $Atm^{D/D}Msh2^{-/-}$ B cells do not have any defects in plasma cell development, Ig production, or Ig secretion.

To determine whether ATM and MSH2 are required for switched Ig isotypes, IgG1 serum concentrations were quantified before immunization and 21 d after a primary and booster immunization with NP-CGG (Fig. 1). Consistent with previous reports, IgG1 is absent in $Aicda^{-/-}$ mice and significantly reduced in $Msh2^{-/-}$ mice (average of 1041 μg/ml) (35, 42). $Atm^{-/-}$ mice exhibit a more pronounced reduction in IgG1 (average of 554 μg/ml) as compared with $Msh2^{-/-}$ mice (13, 14). The average IgG1 titer of $Atm^{D/D}$ mice (354 μg/ml) did not differ significantly from $Atm^{-/-}$ mice pre- or postimmunization, suggesting that the conditional deletion of Atm effectively recapitulates the IgG1 phenotype observed in the germline deletion of Atm. To determine whether the reduced IgG1 resulted from defective germinal center B cell development, Peyer's patches from NP-CGG–immunized mice were stained with anti-B220 Ab and peanut agglutinin and analyzed by flow cytometry (Supplemental Fig. 1A). $Atm^{D/D}Msh2^{-/-}$ mice showed comparable germinal center B cell numbers as compared with WT, $Atm^{D/D}$, and $Msh2^{-/-}$ mice, suggesting that the reduced IgG1 in $Atm^{D/D}Msh2^{-/-}$ mice was not a result of defective germinal center formation but rather a B cell dysfunction in CSR.

To investigate whether $Atm^{D/D}Msh2^{-/-}$ B cells contain an intrinsic defect in CSR, $Atm^{D/D}Msh2^{-/-}$ and control splenic B cells were purified and stimulated in vitro with LPS + IL-4 to induce CSR to

Table III. Genotypes of progeny at day of birth

Cross	N	Genotype	Expected	Observed	χ^2 p Value
$Atm^{+/-}Msh2^{+/-}$	61	$Atm^{+/+}Msh2^{-/-}$	7.625	9	0.292
×		$Atm^{+/+}Msh2^{+/-}$	7.625	9	
$Atm^{+/-}Msh2^{-/-}$		$Atm^{+/-}Msh2^{+/-}$	15.25	19	
		$Atm^{+/-}Msh2^{-/-}$	15.25	13	
		$Atm^{-/-}Msh2^{+/-}$	7.625	9	
		$Atm^{-/-}Msh2^{-/-}$	7.625	2	

The numbers of expected and observed newborn progeny (P0) that were obtained from $Atm^{+/-}Msh2^{+/-} \times Atm^{+/-}Msh2^{-/-}$ crosses in three or more litters are shown. The p value was determined by a χ^2 test.

FIGURE 1. $Atm^{D/D}Msh2^{-/-}$ mice show significantly reduced serum IgG1 titers. Serum titers of IgM and IgG1 were assayed before or after immunization with NP-CGG. Statistical analysis was conducted by one-way ANOVA for $n \geq 5$ mice per genotype in at least four independent experiments (**$p <$ 0.005, ****$p < 0.00001$ as compared with WT). The error bars indicate mean and SD.
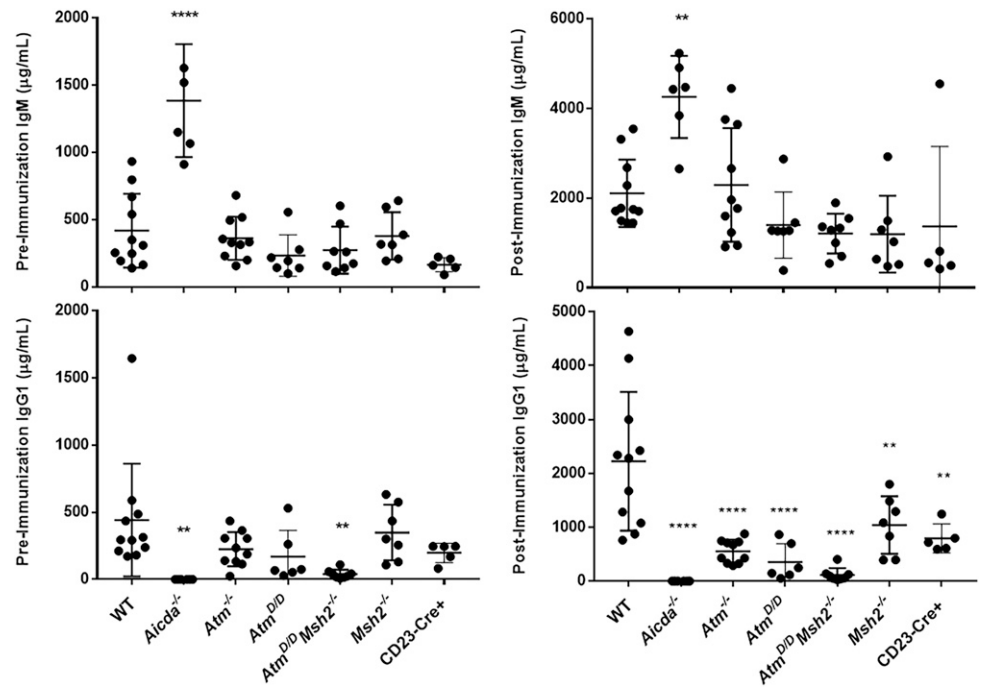
IgG1. Consistent with previous reports (4, 22, 42), CSR to IgG1 is significantly reduced in $Atm^{-/-}$ and $Msh2^{-/-}$ B cells (Fig. 2). However, trace amounts of ATM protein are detectable by immunoblot in $Atm^{D/D}$ B cells (Supplemental Fig. 1B). Additionally, $Atm^{D/D}$ and $Atm^{-/-}$ B cells show no significant difference in CSR to IgG1 ($p = 0.990$). Furthermore, $CD23$-Cre^+ B cells have no significant difference in IgG1 CSR as compared with WT cells ($p = 0.999$), demonstrating that the defect in CSR is not due to aberrant B cell–specific expression of Cre recombinase. As observed in the serum IgG1 of $Atm^{D/D}Msh2^{-/-}$ mice postimmunization (Fig. 1), $Atm^{D/D}$ $Msh2^{-/-}$ B cells exhibit significantly reduced, but not ablated, IgG1 (Fig. 2, $p < 0.0001$). $Atm^{D/D}Msh2^{-/-}$ mouse IgG3 serum titers and $Atm^{D/D}Msh2^{-/-}$ B cells that were stimulated to switch to

IgG3 were similarly reduced (Supplemental Fig. 2), indicating that the defects in CSR in $Atm^{D/D}Msh2^{-/-}$ mice and B cells are not isotype specific. To determine whether the reduction in IgG1 was due to reduced proliferation, $Atm^{D/D}Msh2^{-/-}$ or control B cells were labeled with the far-red dye SNARF 24 h after purification and monitored every 24 h thereafter for dilution of the dye via flow cytometry. No significant differences in cell proliferation were observed between WT, $Atm^{D/D}$, $Msh2^{-/-}$, and $Atm^{D/D}Msh2^{-/-}$ B cells (Supplemental Fig. 3A). $CD23$-Cre^+ B cells diluted the SNARF dye quicker than WT B cells, indicating faster proliferation of $CD23$-Cre^+ B cells (Supplemental Fig. 3A). To examine whether the reduction in IgG1 in $Atm^{D/D}Msh2^{-/-}$ B cells was due to defects in germline transcription at the recombining S regions (47), germline transcripts for μ and γ1 were quantified from LPS + IL-4–stimulated $Atm^{D/D}Msh2^{-/-}$ or control B cells. No significant difference in μ and γ1 germline transcripts was observed across genotypes (Supplemental Fig. 3B, 3C), suggesting that the reduction in CSR observed in $Atm^{D/D}Msh2^{-/-}$ B cells is not due to transcriptional defects. Furthermore, immunoblots for AID showed that $Atm^{D/D}Msh2^{-/-}$ B cells expressed AID comparably to WT, $Atm^{D/D}$, and $Msh2^{-/-}$ B cells (Supplemental Fig. 1B, 1C), indicating that the CSR defect in $Atm^{D/D}Msh2^{-/-}$ B cells is not due to the absence of AID. In sum, the reduced CSR in $Atm^{D/D}Msh2^{-/-}$ B cells likely results from defects in the molecular pathways regulating the formation or repair of DSBs in S regions rather than in plasma cell development, B cell proliferation, transcriptional activation of recombining S regions, or AID expression.

$Atm^{D/D}Msh2^{-/-}$ B cells exhibit defects in NHEJ

CSR occurs through an intrachromosomal recombination between repetitive, intronic S regions that precede each constant coding exon, resulting in the expression of a new Ig isotype and deletion of the intervening constant exons (10). Ligation of the DSBs in the recombining S regions requires an end-joining pathway to repair the DSB and complete the recombination. In WT B cells, end joining during CSR requires primarily NHEJ wherein recombined S−S junctions are ligated with no or a few nucleotides of homology (<4 nt) (48). However, in the absence of NHEJ, B cells completing CSR can use
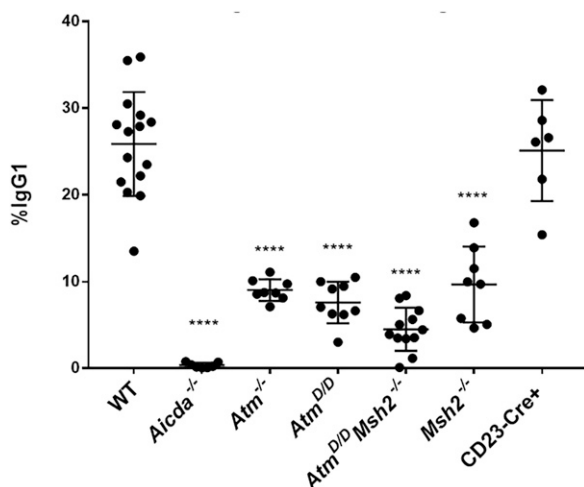
FIGURE 2. $Atm^{D/D}Msh2^{-/-}$ B cells show significantly reduced CSR in vitro. Purified B cells of the indicated genotype were stimulated with LPS + IL-4 to induce CSR to IgG1, which was measured by flow cytometry. Single-cell lymphocytes were identified using forward scatter, side scatter area, side scatter width, and DAPI⁻. Statistical analysis was conducted by one-way ANOVA for $n \geq 6$ mice per genotype in at least four independent experiments (****$p < 0.0001$ as compared with WT). The error bars indicate mean and SD.

an A-EJ pathway that requires resection of the broken DNA to generate short regions of ≥5 nt of homology at the recombined S–S junction (40, 48, 49). Therefore, sequencing the recombined S–S junctions analyzes and quantifies the type of DNA repair and end-joining pathway that is used in recombining S regions. During end joining, the activity of ATM coupled with the amount of DNA resection at the site of recombination determines whether NHEJ will be activated (50, 51). $Atm^{-/-}$ B cells show a reduction in blunt end joins and an increase in microhomologies >4 nt in S–S junctions, suggesting that ATM drives NHEJ during CSR (22). In contrast, S–S junctions from $Msh2^{-/-}$ B cells are joined using blunt or limited microhomology, suggesting that MSH2 promotes A-EJ (10).

To determine whether NHEJ or A-EJ functions in the absence of ATM and MSH2, we analyzed Sμ–Sγ1 junctions from WT, $Atm^{D/D}$, $Msh2^{-/-}$, and $Atm^{D/D}Msh2^{-/-}$ B cells that were stimulated with LPS + IL-4 to induce CSR to IgG1 in vitro (Fig. 3). Sμ–Sγ1 junctions from $Msh2^{-/-}$ B cells contained primarily blunt end joins or short-stretch microhomology, as previously described for Sμ–Sγ3 junctions in $Msh2^{-/-}$ B cells (10, 11, 52). Consistent with Sμ–Sγ1 junctions from $Atm^{-/-}$ B cells (22), Sμ–Sγ1 junctions from $Atm^{D/D}$ B cells trend toward longer stretches of microhomology and reduced blunt joins as compared with WT B cells (Fig. 3A), although these trends have not reached statistical significance. Almost 20% of the Sμ–Sγ1 junctions in $Atm^{D/D}Msh2^{-/-}$ B cells have microhomology lengths of ≥5 nt (Fig. 3A). Most strikingly, Sμ–Sγ1 junctions from $Atm^{D/D}Msh2^{-/-}$ B cells show a significant loss in blunt end joins (Fig. 3A $p = 0.007$), suggesting a severe block in NHEJ in $Atm^{D/D}Msh2^{-/-}$ B cells. Additionally, coupled with the reduction in blunt end joins, $Atm^{D/D}Msh2^{-/-}$ B cells display a stark increase in insertions at Sμ–Sγ1 junctions as compared with WT B cells (Fig. 3A, $p = 0.021$). Significant differences in blunt end joins and insertions are also observed between $Atm^{D/D}Msh2^{-/-}$ and $Msh2^{-/-}$ B cells ($p = 0.001$ and $p = 0.003$, respectively). Although we observed a smaller total percentage of insertions at Sμ–Sγ1 junctions in $Msh2^{-/-}$ B cells as compared with previous Sμ–Sγ3 analysis (10), these insertions were more than triple the length of that observed in WT Sμ–Sγ1 junctions (Fig. 3B). The average inserted sequence at Sμ–Sγ1 junctions in $Msh2^{-/-}$ B cells was 80 nt as compared with 12 nt in WT B cells. Similarly, $Atm^{D/D}$ insertion lengths were longer (average 55 nt) (Fig. 3B). Interestingly, the Sμ–Sγ1 junctions in the $Atm^{D/D}Msh2^{-/-}$ B cells skew toward insertion lengths of ≥100 nt, with the largest insertion size of almost 400 nt; however, the average insertion lengths in Sμ–Sγ1 junctions of $Atm^{D/D}Msh2^{-/-}$ B cells was

not statistically different from the average insertion lengths in $Atm^{D/D}$ and $Msh2^{-/-}$ Sμ–Sγ1 junctions. The significant loss of blunt end joins coupled with an increase in insertions observed in Sμ–Sγ1 junctions of $Atm^{D/D}Msh2^{-/-}$ B cells indicates that MSH2 enforces blunt end joining in the absence of ATM and identifies a distinct recombinogenic repair in $Atm^{D/D}Msh2^{-/-}$ B cells as compared with $Atm^{D/D}$ or $Msh2^{-/-}$ B cells. Collectively, these data suggest that the DSBs in $Atm^{D/D}Msh2^{-/-}$ S regions are joined in a process even more inefficient than either NHEJ or A-EJ that result in an inefficient and sloppy end joining (Fig. 4).

Discussion

Phosphorylation of AID and the subsequent interaction of pS38-AID with APE1 depends on ATM (18), suggesting that ATM may regulate CSR through BER. Based on genetic crosses that inactivated BER and MMR (8), genetic inactivation of Atm and $Msh2$ was predicted to block both BER and MMR pathways, respectively, and abrogate CSR. Surprisingly, dihybrid crosses of $Atm^{+/-}Msh2^{+/-}$ yielded no adult $Atm^{-/-}Msh2^{-/-}$ mice, suggesting a synthetic lethal interaction between mutations in Atm and $Msh2$ (Table I). However, $Msh2^{-/-}$ mice with a conditional deletion of Atm in B cells ($Atm^{D/D}Msh2^{-/-}$) are viable in adulthood, indicating that the $Atm^{-/-}Msh2^{-/-}$ lethality is not B cell–dependent. Although the loss of Atm and $Msh2$ induces a late embryonic to early postnatal lethal phenotype in mice (Tables II, III), the underlying cellular mechanism behind this lethality remains unknown. Synthetic lethality results when the simultaneous loss of two genes leads to cell death, whereas the loss of each gene alone is tolerated and the cells are viable (53–55). In mice, synthetic lethalities between genes encoding DNA damage response proteins usually occur during gestation and early postnatally (56–60). For example, mutations in the genes for the DNA-dependent protein kinase catalytic subunit (DNA-PKcs) and ATM lead to a synthetic lethal phenotype and death of mouse embryos at E7 (61). Interestingly, loss of XRCC4 or DNA ligase IV results in a late embryonic lethality similar to the $Atm^{-/-}Msh2^{-/-}$ embryos (62, 63). The significant loss of blunt end joins in $Atm^{D/D}Msh2^{-/-}$ B cells suggests a block in NHEJ in the absence of ATM and MSH2 (Fig. 3A). However, whether ATM- and MSH2-deficient mouse embryos exhibit any defects in genomic instability and consequently cell proliferation, cell cycle arrest, or cell death remains to be determined. Alternatively, the reduction in observed $Atm^{-/-}Msh2^{-/-}$ mice could result from metabolic defects. ATM and MSH2 respond directly or
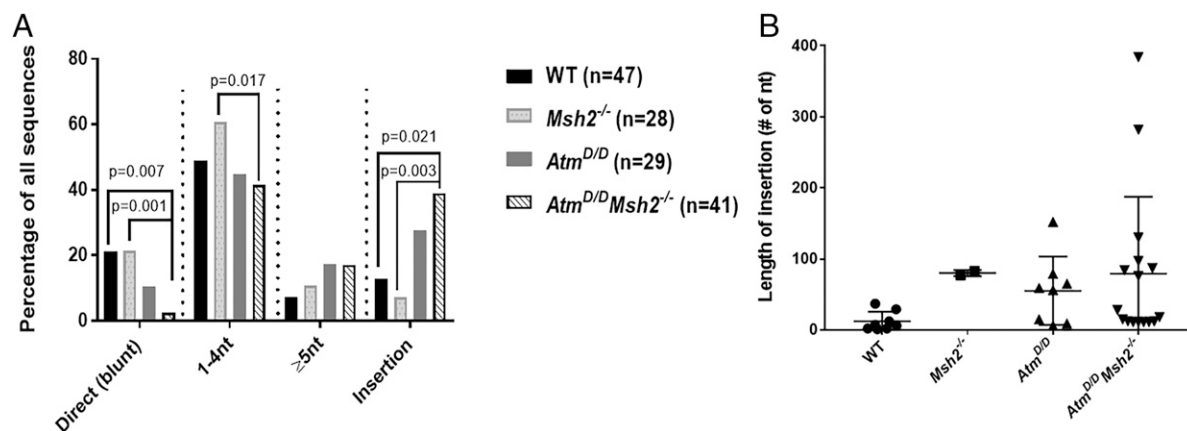
FIGURE 3. Significant loss of blunt end joins and increased insertions in $Atm^{D/D}Msh2^{-/-}$ B cells undergoing CSR to IgG1. (**A**) Percentage of Sμ–Sγ1 junctions with blunt end join (0 nt overlap), 1–4 nt microhomology, ≥5 nt microhomology, or insertion for the indicated genotype. Statistical analysis was conducted using a pairwise t test with a Holm–Sidak correction. Reported p values are unadjusted. (**B**) Length of insertions in Sμ–Sγ1 junctions for the indicated genotype. The error bars indicate mean and SD ($n \geq 3$ mice for each genotype in at least three independent experiments). No statistical difference was observed by one-way ANOVA.
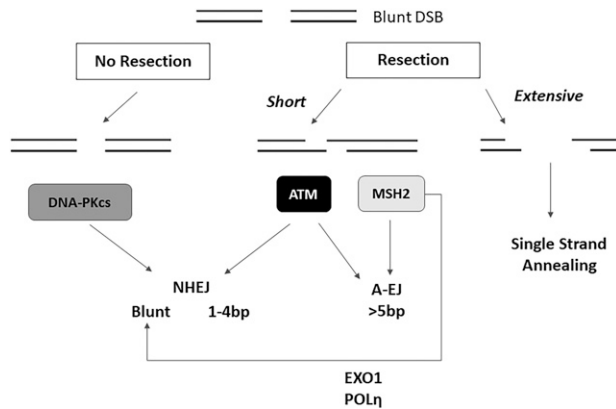
FIGURE 4. Model for the MSH2 enforcement of blunt end joining in the absence of ATM. In NHEJ, blunt end joins are repaired through DNA-PKcs. However, when DSBs are resected, NHEJ repair is mediated by ATM. In the absence of ATM, DSB density is reduced and requires MSH2-dependent SSB conversion by EXO1 or polymerase (POLη). In the absence of ATM and MSH2, resected DNA may also be repaired through SSA due to the extensive DNA resection.

indirectly to reactive oxidative species (ROS), which are produced as byproducts of respiration (64, 65). $Atm^{-/-}$ cells contain higher levels of intracellular ROS as compared with WT cells, and the mechanism by which ATM responds to ROS is independent of its role in DSBs (66, 67). Additionally, MSH2-deficient cells have increased 8-oxo-G–containing DNA, a byproduct of oxidative damage (68). Thus, the synthetic lethality between *Atm* and *Msh2* may result from cellular respiratory failure or mitochondrial damage.

Contrary to the original hypothesis, $Atm^{D/D}Msh2^{-/-}$ B cells complete CSR, albeit at severely impaired levels (Fig. 2, Supplemental Fig. 2A). These data suggest that ATM functions epistatically to BER and MMR during CSR. Alternatively, ATM may be dispensable for BER-driven CSR. Interestingly, $Atm^{-/-}Ung^{-/-}$ mice develop to adulthood and are obtained at Mendelian frequencies (data not shown). $Atm^{-/-}Ung^{-/-}$ mouse IgG1 titers are comparable to $Atm^{-/-}$ mouse IgG1 titers (data not shown), further supporting an epistatic role for ATM. Contrary to the hypothesized role of ATM modulating BER through pS38-AID and APE1, IgG1 titers in $Atm^{D/D}Msh2^{-/-}$ mice were significantly reduced pre- and postimmunization but not ablated (Fig. 1, Supplemental Fig. 2B). To examine the DNA repair pathway used in the absence of ATM and MSH2, Sμ−Sγ1 junctions were sequenced in $Atm^{D/D}Msh2^{-/-}$ B cells that were stimulated to switch to IgG1. Despite the smaller sample size from Sanger sequencing (Fig. 3), the Sμ−Sγ1 junction data are comparable to a high-throughput genome-wide sequencing of stimulated B cells (69) and confirms that ATM promotes NHEJ of S−S junctions in IgG1-switched B cells. Previous work in MSH2-deficient B cells stimulated with LPS indicated an absence of long microhomologies, suggesting a role for MMR in driving A-EJ (10). In contrast to the Sμ−Sγ3 junctions (10), $Msh2^{-/-}$ B cells show Sμ−Sγ1 junctions that are comparable to WT B cells (Fig. 3A). A possible explanation for the discrepancy in the phenotypes reported between Sμ−Sγ3 and Sμ−Sγ1 is that Sγ3 and Sγ1 have different recombination phenotypes in the absence of MSH2, possibly due to different repeat sequences (2, 52, 70). However, in the absence of the NHEJ factor XRCC4, ablating MMR further decreases CSR, supporting the hypothesis that MMR can drive A-EJ (24). Interestingly, the reduced CSR in B cells doubly deficient for XRCC4 and MSH2 is comparable to CSR in the $Atm^{D/D}Msh2^{-/-}$ B cells (Fig. 2, Supplemental Fig. 2A) (24). Furthermore, blunt end joins in Sμ−Sγ1 junctions of $Atm^{D/D}Msh2^{-/-}$ B cells are almost negligible, which indicates a block in NHEJ (Fig. 3A) and is consistent with the phenotype observed in the NHEJ-deficient $Xrcc4^{-/-}$ B cells

(24). Collectively, this would suggest that MSH2 may enforce blunt end joining in the absence of NHEJ (24). Previously, Stavnezer and Schrader (71) proposed a model wherein MSH2 functions to convert staggered SSBs into DSBs through end processing of distal C residues on opposite strands, either by 3′ loading of EXO1 to the MMR complex (72, 73) or through the recruitment of DNA polymerase η by MSH2/MSH6 to synthesize nucleotides at resected SSBs until a blunt DSB has been reached (74). Following this model of MSH2-dependent DSB conversion, perhaps the presence or absence of ATM determines the density of DSBs within a recombining S region, possibly through the recruitment of APE1 by ATM-dependent phosphorylation of AID (18). Thus, in the absence of ATM fewer DSBs are generated, constituting the need for MSH2 blunt end joining. Speculatively, NHEJ and A-EJ may function suboptimally in ATM- and MSH2-deficient B cells to create a heterogeneous phenotype in end joining where the absence of ATM and MSH2 exerts an epistatic suppression of NHEJ, which may account for the reduction in blunt joins.

Alternatively, other NHEJ proteins may compensate for the absence of ATM (61, 75). During V(D)J recombination, which utilizes NHEJ at conserved recombination signal sequences cleaved by RAG1/2, NHEJ is driven mostly by DNA-PKcs (76–78). ATM participates in the repair of RAG-induced DSBs; however, it is insufficient to rescue NHEJ during V(D)J recombination in the absence of DNA-PKcs (79, 80). Interestingly, MSH2 is dispensable for NHEJ in V(D)J recombination despite its known involvement in CSR (81), suggesting that although both CSR and V(D)J use NHEJ, there remain uncharacterized mechanistic differences between the processes. In CSR, DNA-PKcs can partially function in NHEJ in the absence of ATM (82), which could account for the lack of significant difference in the percentage of short stretches of microhomologies (1–4 nt) in $Atm^{D/D}Msh2^{-/-}$ B cells as compared with the control genotypes (Fig. 3). However, the extent to which DNA-PKcs can compensate for the absence of ATM may depend on the amount of resection at the broken ends. When limited resection of DSB ends has occurred, the Ku70/80 complex efficiently binds the DSB (83), which allows for recruitment of DNA-PKcs, Artemis, XRCC4, and LigIV to efficiently join the broken ends through NHEJ (84, 85). Because the Ku complex has low affinity for resected DNA (86), the initiation of resection is a critical determinant for repair pathway choice. Interestingly, there is evidence to suggest that A-EJ driven by resection occurs in CSR. RPA, a ssDNA-binding protein that regulates DNA resection (87, 88), interacts with pS38-AID at S regions (19). Furthermore, B cells defective in 53BP1 exhibit an increase in ATM-mediated end resection that is repaired through A-EJ during CSR (89). Interestingly, $Atm^{D/D}Msh2^{-/-}$ B cells show an increased percentage of Sμ−Sγ1 junctions with insertions, many of which are some of the longest in length (up to 380 bp) across all of the assayed genotypes (Fig. 3B). This phenotype is comparable to that observed in the absence of 53BP1, suggesting that $Atm^{D/D}Msh2^{-/-}$ insertions may have an increase in end resections that have not been repaired through A-EJ. An alternative explanation for the increased insertions could be that the absence of ATM and MSH2 leads to an increase in resection with no mechanism to repair through NHEJ or A-EJ and thus requires the need for a salvage pathway. Single strand annealing (SSA) has been observed in yeast in the case of resected DNA homology-based repair but in the absence of functional HR, leading to high rates of mutagenesis (90–92). In this way, the increase in insertions observed in $Atm^{D/D}Msh2^{-/-}$ B cells may indicate an attempt at salvage repair through SSA. Additionally, members of the SAGA (Spt-Ada-Gcn5-acetyltransferase) deubiquitylation complex such as USP22, ENY2, and ATXN7 may modulate NHEJ, A-EJ, and SSA during CSR (93); however, the role of ATM and MSH2 in regulating SAGA remains unknown. Collectively, this may indicate

that ATM and MSH2 are required to repair resected DNA to drive A-EJ (Fig. 4).

We hypothesize that pS38-AID–mediated interaction with RPA-coated resected ssDNA may signal through ATM in a positive feedback loop to increase the density of resected DNA breaks in recombining S regions (18, 94). We propose a model whereby the phosphorylation of AID through an uncharacterized ATM–protein kinase A signaling cascade activates A-EJ in CSR (Fig. 4). Hypothetically, in the absence of resection (i.e., blunt end joins), the Ku complex efficiently binds the broken ends and recruits DNA-PKcs–mediated NHEJ. However, when the DSB ends have been resected, NHEJ is driven by ATM. In the absence of ATM, MSH2 promotes the conversion of staggered SSBs into DSBs through the recruitment of either EXO1 or polymerase η to generate blunt ends that can be joined through NHEJ. We speculate that activation of ATM indirectly induces the phosphorylation of S38 on AID, which in turn may cointeract with resected SSB coated by RPA (95), facilitating microhomology-mediated strand invasion into the acceptor S region to complete repair through A-EJ. In the absence of ATM and MSH2, resected DNA may also be repaired through SSA due to the extensive resection.

Acknowledgments

Disclosures

The authors have no financial conflicts of interest.

References

1. Alt, F. W., E. M. Oltz, F. Young, J. Gorman, G. Taccioli, and J. Chen. 1992. VDJ recombination. *Immunol. Today* 13: 306–314.
2. Chaudhuri, J., and F. W. Alt. 2004. Class-switch recombination: interplay of transcription, DNA deamination and DNA repair. [Published erratum appears in 2004 *Nat. Rev. Immunol.* 4: 655.] *Nat. Rev. Immunol.* 4: 541–552.
3. Rush, J. S., S. D. Fugmann, and D. G. Schatz. 2004. Staggered AID-dependent DNA double strand breaks are the predominant DNA lesions targeted to Sμ in Ig class switch recombination. *Int. Immunol.* 16: 549–557.
4. Alt, F. W., Y. Zhang, F.-L. Meng, C. Guo, and B. Schwer. 2013. Mechanisms of programmed DNA lesions and genomic instability in the immune system. *Cell* 152: 417–429.
5. Xu, Z., H. Zan, E. J. Pone, T. Mai, and P. Casali. 2012. Immunoglobulin class-switch DNA recombination: induction, targeting and beyond. *Nat. Rev. Immunol.* 12: 517–531.
6. Methot, S., and J. Di Noia. 2017. Molecular mechanisms of somatic hypermutation and class switch recombination. *Adv. Immunol.* 133: 37–87.
7. Honjo, T., M. Muramatsu, and S. Fagarasan. 2004. AID: how does it aid antibody diversity? *Immunity* 20: 659–668.
8. Rada, C., J. M. Di Noia, and M. S. Neuberger. 2004. Mismatch recognition and uracil excision provide complementary paths to both Ig switching and the A/T-focused phase of somatic mutation. *Mol. Cell* 16: 163–171.
9. Rada, C., G. T. Williams, H. Nilsen, D. E. Barnes, T. Lindahl, and M. S. Neuberger. 2002. Immunoglobulin isotype switching is inhibited and somatic hypermutation perturbed in UNG-deficient mice. *Curr. Biol.* 12: 1748–1755.
10. Schrader, C. E., J. Vardo, and J. Stavnezer. 2002. Role for mismatch repair proteins Msh2, Mlh1, and Pms2 in immunoglobulin class switching shown by sequence analysis of recombination junctions. *J. Exp. Med.* 195: 367–373.
11. Martin, A., Z. Li, D. P. Lin, P. D. Bardwell, M. D. Iglesias-Ussel, W. Edelmann, and M. D. Scharff. 2003. Msh2 ATPase activity is essential for somatic hypermutation at A-T basepairs and for efficient class switch recombination. *J. Exp. Med.* 198: 1171–1178.
12. Imai, K., G. Slupphaug, W.-I. Lee, P. Revy, S. Nonoyama, N. Catalan, L. Yel, M. Forveille, B. Kavli, H. E. Krokan, et al. 2003. Human uracil-DNA glycosylase deficiency associated with profoundly impaired immunoglobulin class-switch recombination. *Nat. Immunol.* 4: 1023–1028.
13. Masani, S., L. Han, and K. Yu. 2013. Apurinic/apyrimidinic endonuclease 1 is the essential nuclease during immunoglobulin class switch recombination. *Mol. Cell. Biol.* 33: 1468–1473.
14. Guikema, J. E., E. K. Linehan, D. Tsuchimoto, Y. Nakabeppu, P. R. Strauss, J. Stavnezer, and C. E. Schrader. 2007. APE1- and APE2-dependent DNA breaks in immunoglobulin class switch recombination. *J. Exp. Med.* 204: 3017–3026.
15. Schrader, C. E., J. E. Guikema, X. Wu, and J. Stavnezer. 2009. The roles of APE1, APE2, DNA polymerase β and mismatch repair in creating S region DNA breaks during antibody class switch. *Philos. Trans. R. Soc. Lond. B Biol. Sci.* 364: 645–652.
16. Seeberg, E., L. Eide, and M. Bjørås. 1995. The base excision repair pathway. *Trends Biochem. Sci.* 20: 391–397.
17. Tishkoff, D. X., A. L. Boerger, P. Bertrand, N. Filosi, G. M. Gaida, M. F. Kane, and R. D. Kolodner. 1997. Identification and characterization of *Saccharomyces cerevisiae EXO1*, a gene encoding an exonuclease that interacts with MSH2. *Proc. Natl. Acad. Sci. USA* 94: 7487–7492.
18. Vuong, B. Q., K. Herrick-Reynolds, B. Vaidyanathan, J. N. Pucella, A. J. Ucher, N. M. Donghia, X. Gu, L. Nicolas, U. Nowak, N. Rahman, et al. 2013. A DNA break- and phosphorylation-dependent positive feedback loop promotes immunoglobulin class-switch recombination. *Nat. Immunol.* 14: 1183–1189.
19. Cheng, H.-L., B. Q. Vuong, U. Basu, A. Franklin, B. Schwer, J. Astarita, R. T. Phan, A. Datta, J. Manis, F. W. Alt, and J. Chaudhuri. 2009. Integrity of the AID serine-38 phosphorylation site is critical for class switch recombination and somatic hypermutation in mice. [Published erratum appears in 2013 *Proc. Natl. Acad. Sci. USA* 5731.] *Proc. Natl. Acad. Sci. USA* 106: 2717–2722.
20. McBride, K. M., A. Gazumyan, E. M. Woo, T. A. Schwickert, B. T. Chait, and M. C. Nussenzweig. 2008. Regulation of class switch recombination and somatic mutation by AID phosphorylation. *J. Exp. Med.* 205: 2585–2594.
21. Choi, J. E., A. J. Matthews, G. Michel, and B. Q. Vuong. 2020. AID phosphorylation regulates mismatch repair-dependent class switch recombination and affinity maturation. *J. Immunol.* 204: 13–22.
22. Reina-San-Martin, B., H. T. Chen, A. Nussenzweig, and M. C. Nussenzweig. 2004. ATM is required for efficient recombination between immunoglobulin switch regions. *J. Exp. Med.* 200: 1103–1110.
23. Lumsden, J. M., T. McCarty, L. K. Petiniot, R. Shen, C. Barlow, T. A. Wynn, H. C. Morse III, P. J. Gearhart, A. Wynshaw-Boris, E. E. Max, and R. J. Hodes. 2004. Immunoglobulin class switch recombination is impaired in *Atm*-deficient mice. *J. Exp. Med.* 200: 1111–1121.
24. Eccleston, J., C. Yan, K. Yuan, F. W. Alt, and E. Selsing. 2011. Mismatch repair proteins MSH2, MLH1, and EXO1 are important for class-switch recombination events occurring in B cells that lack nonhomologous end joining. *J. Immunol.* 186: 2336–2343.
25. Rooney, S., J. Chaudhuri, and F. W. Alt. 2004. The role of the non-homologous end-joining pathway in lymphocyte development. *Immunol. Rev.* 200: 115–131.
26. Boboila, C., C. Yan, D. R. Wesemann, M. Jankovic, J. H. Wang, J. Manis, A. Nussenzweig, M. Nussenzweig, and F. W. Alt. 2010. Alternative end-joining catalyzes class switch recombination in the absence of both Ku70 and DNA ligase 4. [Published erratum appears in 2013 *J. Exp. Med.* 210: 641.] *J. Exp. Med.* 207: 417–427.
27. Yan, C. T., C. Boboila, E. K. Souza, S. Franco, T. R. Hickernell, M. Murphy, S. Gumaste, M. Geyer, A. A. Zarrin, J. P. Manis, et al. 2007. IgH class switching and translocations use a robust non-classical end-joining pathway. *Nature* 449: 478–482.
28. Soulas-Sprauel, P., G. Le Guyader, P. Rivera-Munoz, V. Abramowski, C. Olivier-Martin, C. Goujet-Zalc, P. Charneau, and J.-P. de Villartay. 2007. Role for DNA repair factor XRCC4 in immunoglobulin class switch recombination. *J. Exp. Med.* 204: 1717–1727.
29. Boboila, C., V. Oksenych, M. Gostissa, J. H. Wang, S. Zha, Y. Zhang, H. Chai, C.-S. Lee, M. Jankovic, L.-M. A. Saez, et al. 2012. Robust chromosomal DNA repair via alternative end-joining in the absence of x-ray repair cross-complementing protein 1 (XRCC1). [Published erratum appears in 2013 *Proc. Natl. Acad. Sci. USA* 110: 5731.] *Proc. Natl. Acad. Sci. USA* 109: 2473–2478.
30. Boboila, C., M. Jankovic, C. T. Yan, J. H. Wang, D. R. Wesemann, T. Zhang, A. Fazeli, L. Feldman, A. Nussenzweig, M. Nussenzweig, and F. W. Alt. 2010. Alternative end-joining catalyzes robust IgH locus deletions and translocations in the combined absence of ligase 4 and Ku70. [Published erratum appears in 2013 *Proc. Natl. Acad. Sci. USA* 110: 5731.] *Proc. Natl. Acad. Sci. USA* 107: 3034–3039.
31. Dunnick, W., G. Z. Hertz, L. Scappino, and C. Gritzmacher. 1993. DNA sequences at immunoglobulin switch region recombination sites. *Nucleic Acids Res.* 21: 365–372.
32. Pan, Q., C. Petit-Frére, A. Lähdesmäki, H. Gregorek, K. H. Chrzanowska, and L. Hammarström. 2002. Alternative end joining during switch recombination in patients with ataxia-telangiectasia. *Eur. J. Immunol.* 32: 1300–1308.
33. Barlow, C., S. Hirotsune, R. Paylor, M. Liyanage, M. Eckhaus, F. Collins, Y. Shiloh, J. N. Crawley, T. Ried, D. Tagle, and A. Wynshaw-Boris. 1996. *Atm*-deficient mice: a paradigm of ataxia telangiectasia. *Cell* 86: 159–171.
34. de Wind, N., M. Dekker, A. Berns, M. Radman, and H. te Riele. 1995. Inactivation of the mouse *Msh2* gene results in mismatch repair deficiency, methylation tolerance, hyperrecombination, and predisposition to cancer. *Cell* 82: 321–330.
35. Muramatsu, M., K. Kinoshita, S. Fagarasan, S. Yamada, Y. Shinkai, and T. Honjo. 2000. Class switch recombination and hypermutation require activation-induced cytidine deaminase (AID), a potential RNA editing enzyme. *Cell* 102: 553–563.
36. Zha, S., J. Sekiguchi, J. W. Brush, C. H. Bassing, and F. W. Alt. 2008. Complementary functions of ATM and H2AX in development and suppression of genomic instability. *Proc. Natl. Acad. Sci. USA* 105: 9302–9306.
37. Kwon, K., C. Hutter, Q. Sun, I. Bilic, C. Cobaleda, S. Malin, and M. Busslinger. 2008. Instructive role of the transcription factor E2A in early B lymphopoiesis and germinal center B cell development. *Immunity* 28: 751–762.
38. Chaudhuri, J., M. Tian, C. Khuong, K. Chua, E. Pinaud, and F. W. Alt. 2003. Transcription-targeted DNA deamination by the AID antibody diversification enzyme. *Nature* 422: 726–730.
39. Pucella, J. N., W.-F. Yen, M. V. Kim, J. van der Veeken, C. T. Luo, N. D. Socci, Y. Naito, M. O. Li, N. Iwai, and J. Chaudhuri. 2015. miR-182 is largely dispensable for

adaptive immunity: lack of correlation between expression and function. [Published erratum appears in 2015 *J. Immunol.* 195: 1903.] *J. Immunol.* 194: 2635–2642.

40. Ehrenstein, M. R., C. Rada, A.-M. Jones, C. Milstein, and M. S. Neuberger. 2001. Switch junction sequences in PMS2-deficient mice reveal a microhomology-mediated mechanism of Ig class switch recombination. *Proc. Natl. Acad. Sci. USA* 98: 14553–14558.

41. Zan, H., C. Tat, Z. Qiu, J. R. Taylor, J. A. Guerrero, T. Shen, and P. Casali. 2017. Rad52 competes with Ku70/Ku86 for binding to S-region DSB ends to modulate antibody class-switch DNA recombination. *Nat. Commun.* 8: 14244.

42. Reitmair, A. H., R. Schmits, A. Ewel, B. Bapat, M. Redston, A. Mitri, P. Waterhouse, H.-W. Mittrücker, A. Wakeham, B. Liu, et al. 1995. MSH2 deficient mice are viable and susceptible to lymphoid tumours. *Nat. Genet.* 11: 64–70.

43. Callén, E., M. Jankovic, S. Difilippantonio, J. A. Daniel, H.-T. Chen, A. Celeste, M. Pellegrini, K. McBride, D. Wangsa, A. L. Bredemeyer, et al. 2007. ATM prevents the persistence and propagation of chromosome breaks in lymphocytes. *Cell* 130: 63–75.

44. Aubry, J.-P., S. Pochon, P. Graber, K. U. Jansen, and J.-Y. Bonnefoy. 1992. CD21 is a ligand for CD23 and regulates IgE production. *Nature* 358: 505–507.

45. Shih, T. A., E. Meffre, M. Roederer, and M. C. Nussenzweig. 2002. Role of BCR affinity in T cell dependent antibody responses in vivo. *Nat. Immunol.* 3: 570–575.

46. Toellner, K.-M., W. E. Jenkinson, D. R. Taylor, M. Khan, D. M.-Y. Sze, D. M. Sansom, C. G. Vinuesa, and I. C. MacLennan. 2002. Low-level hypermutation in T cell-independent germinal centers compared with high mutation rates associated with T cell-dependent germinal centers. *J. Exp. Med.* 195: 383–389.

47. Manis, J. P., M. Tian, and F. W. Alt. 2002. Mechanism and control of class-switch recombination. *Trends Immunol.* 23: 31–39.

48. Lee-Theilen, M., A. J. Matthews, D. Kelly, S. Zheng, and J. Chaudhuri. 2011. CtIP promotes microhomology-mediated alternative end joining during class-switch recombination. *Nat. Struct. Mol. Biol.* 18: 75–79.

49. Stavnezer, J., A. Björkman, L. Du, A. Cagigi, and Q. Pan-Hammarström. 2010. Mapping of switch recombination junctions, a tool for studying DNA repair pathways during immunoglobulin class switching. *Adv. Immunol.* 108: 45–109.

50. Bothmer, A., D. F. Robbiani, N. Feldhahn, A. Gazumyan, A. Nussenzweig, and M. C. Nussenzweig. 2010. 53BP1 regulates DNA resection and the choice between classical and alternative end joining during class switch recombination. *J. Exp. Med.* 207: 855–865.

51. Symington, L. S., and J. Gautier. 2011. Double-strand break end resection and repair pathway choice. *Annu. Rev. Genet.* 45: 247–271.

52. Ehrenstein, M. R., and M. S. Neuberger. 1999. Deficiency in Msh2 affects the efficiency and local sequence specificity of immunoglobulin class-switch recombination: parallels with somatic hypermutation. *EMBO J.* 18: 3484–3490.

53. Ashworth, A., C. J. Lord, and J. S. Reis-Filho. 2011. Genetic interactions in cancer progression and treatment. *Cell* 145: 30–38.

54. Farmer, H., N. McCabe, C. J. Lord, A. N. Tutt, D. A. Johnson, T. B. Richardson, M. Santarosa, K. J. Dillon, I. Hickson, C. Knights, et al. 2005. Targeting the DNA repair defect in BRCA mutant cells as a therapeutic strategy. *Nature* 434: 917–921.

55. Bryant, H. E., N. Schultz, H. D. Thomas, K. M. Parker, D. Flower, E. Lopez, S. Kyle, M. Meuth, N. J. Curtin, and T. Helleday. 2005. Specific killing of BRCA2-deficient tumours with inhibitors of poly(ADP-ribose) polymerase. [Published erratum appears in 2007 *Nature* 447: 346.] *Nature* 434: 913–917.

56. Kantidze, O. L., A. K. Velichko, A. V. Luzhin, N. V. Petrova, and S. V. Razin. 2018. Synthetically lethal interactions of ATM, ATR, and DNA-PKcs. *Trends Cancer* 4: 755–768.

57. Daniel, J. A., M. Pellegrini, B.-S. Lee, Z. Guo, D. Filsuf, N. V. Belkina, Z. You, T. T. Paull, B. P. Sleckman, L. Feigenbaum, and A. Nussenzweig. 2012. Loss of ATM kinase activity leads to embryonic lethality in mice. *J. Cell Biol.* 198: 295–304.

58. Ménisser-de Murcia, J., M. Mark, O. Wendling, A. Wynshaw-Boris, and G. de Murcia. 2001. Early embryonic lethality in PARP-1 Atm double-mutant mice suggests a functional synergy in cell proliferation during development. *Mol. Cell. Biol.* 21: 1828–1832.

59. Huber, A., P. Bai, J. M. de Murcia, and G. de Murcia. 2004. PARP-1, PARP-2 and ATM in the DNA damage response: functional synergy in mouse development. *DNA Repair (Amst.)* 3: 1103–1108.

60. Sekiguchi, J., D. O. Ferguson, H. T. Chen, E. M. Yang, J. Earle, K. Frank, S. Whitlow, Y. Gu, Y. Xu, A. Nussenzweig, and F. W. Alt. 2001. Genetic interactions between ATM and the nonhomologous end-joining factors in genomic stability and development. *Proc. Natl. Acad. Sci. USA* 98: 3243–3248.

61. Gurley, K. E., and C. J. Kemp. 2001. Synthetic lethality between mutation in Atm and DNA-PK(cs) during murine embryogenesis. *Curr. Biol.* 11: 191–194.

62. Gao, Y., Y. Sun, K. M. Frank, P. Dikkes, S. Fujiwara, K. J. Seidl, J. M. Sekiguchi, G. A. Rathbun, W. Swat, J. Wang, et al. 1998. A critical role for DNA end-joining proteins in both lymphogenesis and neurogenesis. *Cell* 95: 891–902.

63. Frank, K. M., N. E. Sharpless, Y. Gao, J. M. Sekiguchi, D. O. Ferguson, C. Zhu, J. P. Manis, J. Horner, R. A. DePinho, and F. W. Alt. 2000. DNA ligase IV deficiency in mice leads to defective neurogenesis and embryonic lethality via the p53 pathway. *Mol. Cell* 5: 993–1002.

64. Kozlov, S. V., A. J. Waardenberg, K. Engholm-Keller, J. W. Arthur, M. E. Graham, and M. Lavin. 2016. Reactive oxygen species (ROS)-activated ATM-dependent phosphorylation of cytoplasmic substrates identified by large-scale phosphoproteomics screen. *Mol. Cell. Proteomics* 15: 1032–1047.

65. Martin, S. A., N. McCabe, M. Mullarkey, R. Cummins, D. J. Burgess, Y. Nakabeppu, S. Oka, E. Kay, C. J. Lord, and A. Ashworth. 2010. DNA polymerases as potential therapeutic targets for cancers deficient in the DNA mismatch repair proteins MSH2 or MLH1. *Cancer Cell* 17: 235–248.

66. Ito, K., K. Takubo, F. Arai, H. Satoh, S. Matsuoka, K. Ohmura, K. Naka, M. Azuma, K. Miyamoto, K. Hosokawa, et al. 2007. Regulation of reactive oxygen

67. Guo, Z., S. Kozlov, M. F. Lavin, M. D. Person, and T. T. Paull. 2010. ATM activation by oxidative stress. *Science* 330: 517–521.

68. Colussi, C., E. Parlanti, P. Degan, G. Aquilina, D. Barnes, P. Macpherson, P. Karran, M. Crescenzi, E. Dogliotti, and M. Bignami. 2002. The mammalian mismatch repair pathway removes DNA 8-oxodGMP incorporated from the oxidized dNTP pool. *Curr. Biol.* 12: 912–918.

69. Panchakshari, R. A., X. Zhang, V. Kumar, Z. Du, P.-C. Wei, J. Kao, J. Dong, and F. W. Alt. 2018. DNA double-strand break response factors influence end-joining features of IgH class switch and general translocation junctions. *Proc. Natl. Acad. Sci. USA* 115: 762–767.

70. Min, I. M., C. E. Schrader, J. Vardo, T. M. Luby, N. D'Avirro, J. Stavnezer, and E. Selsing. 2003. The Sμ tandem repeat region is critical for Ig isotype switching in the absence of Msh2. *Immunity* 19: 515–524.

71. Stavnezer, J., and C. E. Schrader. 2006. Mismatch repair converts AID-instigated nicks to double-strand breaks for antibody class-switch recombination. *Trends Genet.* 22: 23–28.

72. Bardwell, P. D., C. J. Woo, K. Wei, Z. Li, A. Martin, S. Z. Sack, T. Parris, W. Edelmann, and M. D. Scharff. 2004. Altered somatic hypermutation and reduced class-switch recombination in exonuclease 1-mutant mice. *Nat. Immunol.* 5: 224–229.

73. Genschel, J., and P. Modrich. 2003. Mechanism of 5′-directed excision in human mismatch repair. *Mol. Cell* 12: 1077–1086.

74. Wilson, T. M., A. Vaisman, S. A. Martomo, P. Sullivan, L. Lan, F. Hanaoka, A. Yasui, R. Woodgate, and P. J. Gearhart. 2005. MSH2–MSH6 stimulates DNA polymerase η, suggesting a role for A:T mutations in antibody genes. *J. Exp. Med.* 201: 637–645.

75. Callén, E., M. Jankovic, N. Wong, S. Zha, H.-T. Chen, S. Difilippantonio, M. Di Virgilio, G. Heidkamp, F. W. Alt, A. Nussenzweig, and M. Nussenzweig. 2009. Essential role for DNA-PKcs in DNA double-strand break repair and apoptosis in ATM-deficient lymphocytes. *Mol. Cell* 34: 285–297.

76. Oettinger, M. A., D. G. Schatz, C. Gorka, and D. Baltimore. 1990. RAG-1 and RAG-2, adjacent genes that synergistically activate V(D)J recombination. *Science* 248: 1517–1523.

77. Bassing, C. H., W. Swat, and F. W. Alt. 2002. The mechanism and regulation of chromosomal V(D)J recombination. *Cell* 109(Suppl.): S45–S55.

78. Hefferin, M. L., and A. E. Tomkinson. 2005. Mechanism of DNA double-strand break repair by non-homologous end joining. *DNA Repair (Amst.)* 4: 639–648.

79. Bredemeyer, A. L., G. G. Sharma, C.-Y. Huang, B. A. Helmink, L. M. Walker, K. C. Khor, B. Nuskey, K. E. Sullivan, T. K. Pandita, C. H. Bassing, and B. P. Sleckman. 2006. ATM stabilizes DNA double-strand-break complexes during V(D)J recombination. *Nature* 442: 466–470.

80. Blunt, T., N. J. Finnie, G. E. Taccioli, G. C. Smith, J. Demengeot, T. M. Gottlieb, R. Mizuta, A. J. Varghese, F. W. Alt, P. A. Jeggo, and S. P. Jackson. 1995. Defective DNA-dependent protein kinase activity is linked to V(D)J recombination and DNA repair defects associated with the murine scid mutation. *Cell* 80: 813–823.

81. Larijani, M., A. Zaheen, D. Frieder, Y. Wang, G. E. Wu, W. Edelmann, and A. Martin. 2005. Lack of MSH2 involvement differentiates V(D)J recombination from other nonhomologous end joining events. *Nucleic Acids Res.* 33: 6733–6742.

82. Cook, A. J., L. Oganesian, P. Harumal, A. Basten, R. Brink, and C. J. Jolly. 2003. Reduced switching in SCID B cells is associated with altered somatic mutation of recombined S regions. *J. Immunol.* 171: 6556–6564.

83. Ira, G., A. Pellicioli, A. Balijja, X. Wang, S. Fiorani, W. Carotenuto, G. Liberi, D. Bressan, L. Wan, N. M. Hollingsworth, et al. 2004. DNA end resection, homologous recombination and DNA damage checkpoint activation require CDK1. *Nature* 431: 1011–1017.

84. Blackford, A. N., and S. P. Jackson. 2017. ATM, ATR, and DNA-PK: the trinity at the heart of the DNA damage response. *Mol. Cell* 66: 801–817.

85. Falck, J., J. Coates, and S. P. Jackson. 2005. Conserved modes of recruitment of ATM, ATR and DNA-PKcs to sites of DNA damage. *Nature* 434: 605–611.

86. Dynan, W. S., and S. Yoo. 1998. Interaction of Ku protein and DNA-dependent protein kinase catalytic subunit with nucleic acids. *Nucleic Acids Res.* 26: 1551–1559.

87. Chen, H., M. Lisby, and L. S. Symington. 2013. RPA coordinates DNA end resection and prevents formation of DNA hairpins. *Mol. Cell* 50: 589–600.

88. Soniat, M. M., L. R. Myler, H.-C. Kuo, T. T. Paull, and I. J. Finkelstein. 2019. RPA phosphorylation inhibits DNA resection. *Mol. Cell* 75: 145–153.e5.

89. Reina-San-Martin, B., J. Chen, A. Nussenzweig, and M. C. Nussenzweig. 2007. Enhanced intra-switch region recombination during immunoglobulin class switch recombination in 53BP1−/− B cells. *Eur. J. Immunol.* 37: 235–239.

90. Weinstock, D. M., C. A. Richardson, B. Elliott, and M. Jasin. 2006. Modeling oncogenic translocations: distinct roles for double-strand break repair pathways in translocation formation in mammalian cells. *DNA Repair (Amst.)* 5: 1065–1074.

91. Moynahan, M. E., and M. Jasin. 2010. Mitotic homologous recombination maintains genomic stability and suppresses tumorigenesis. *Nat. Rev. Mol. Cell Biol.* 11: 196–207.

92. Spies, M., and R. Fishel. 2015. Mismatch repair during homologous and homeologous recombination. *Cold Spring Harb. Perspect. Biol.* 7: a022657.

93. Li, C., T. Irrazabal, C. C. So, M. Berru, L. Du, E. Lam, A. K. Ling, J. L. Gommerman, Q. Pan-Hammarström, and A. Martin. 2018. The H2B deubiquitinase Usp22 promotes antibody class switch recombination by facilitating non-homologous end joining. *Nat. Commun.* 9: 1006.

94. Matthews, A. J., S. Zheng, L. J. DiMenna, and J. Chaudhuri. 2014. Regulation of immunoglobulin class-switch recombination: choreography of noncoding transcription, targeted DNA deamination, and long-range DNA repair. *Adv. Immunol.* 122: 1–57.

95. Yamane, A., D. F. Robbiani, W. Resch, A. Bothmer, H. Nakahashi, T. Oliveira, P. C. Rommel, E. J. Brown, A. Nussenzweig, M. C. Nussenzweig, and R. Casellas. 2013. RPA accumulation during class switch recombination represents 5′-3′ DNA-end resection during the S-G2/M phase of the cell cycle. *Cell Rep.* 3: 138–147.